Arrangement of Cables in Cable Stayed Bridges with Various Pylon Shapes and Connection Types

Mohamed Naguib[1], Saher R. Elkhoriby[2], Mahmoud H. El-Boghdadi[3], Salah S. El-Stohey[4]

[1] Professor, Civil Engineering Department, Faculty of Engineering, Mansoura University, Mansoura, Egypt, naguib2005@yahoo.com
[2] Professor, Civil Engineering Department, Faculty of Engineering, Tanta University, Tanta, Egypt, saher.ibrahim@f-eng.tanta.edu.eg
[3] Associate. Professor, Civil Engineering Department, Faculty of Engineering, Tanta University, Tanta, Egypt, mahmoud.el-boghdadi@f-eng.tanta.edu.eg
4 Civil Engineering Department, Nile Higher Institute for Engineering & Technology, Mansoura, Egypt, salahsaad220@gmail.com

Abstract-The cable-stayed bridges (CSBs) had become the most important structure for long span bridges. Modern cable stayed bridges are more acceptable and flexible enough to resist wind and traffic loads. A typical cable-stayed bridge has a deck with a number of pylons and cables arranged in harp, radiating, and semi-fan bridge configurations. The bridges' static analysis was carried out using a FORTRAN finite element program based on the minimization of Total Potential Energy "TPE" applying the method of conjugate gradient [1]. The analysis is carried out for five spans CSBs with considering three shapes of pylons H, A and Y shape. Four popular connection cases have been shown to describe the effect of connections between pylons and floor beams. The effect of initial tension in cables and various heights of pylons are taken into consideration as parametric study. Also all above requirements are applied on Harp, Radiating, and Semi-Fan bridges.

Keywords: Cable arrangement, Cable stayed, Bridges, Pylon shape, connection, initial tension.

I. INTRODUCTION

Cable stayed bridge is known as the bridge that has one or more towers from which cables support the floor beam. A large amount of compression forces transfers from the deck to foundations through cables and pylons. Cable-stayed bridges are effective in resisting earthquakes. It provides an outstanding architectural appearance due to their small diameter cables and unique overhead structure. Using large computers, the static and dynamic analysis of those types of bridges became easy to choose the optimum design taking in mind the financial part.

The most common types of cable arrangements are harp, radiating and semi fan bridges. The various possible types of tower construction may take the form of: A-Shape, Diamond Shape, H-shape, Trapezoidal portal frames (modified A-shape), Single plane tower, Y-shape and Inverted Y-shape.

A comparison between three arrangement types, in terms of lateral displacement, vertical deflection, normal force and bending moment is carried out. A cable stayed bridge (CBS) is analyzed by changing the cables' arrangement with different shapes of pylons. The three cables' arrangement taken is harp, radiating and semi fan arrangement. The pylons are of two laterals of stays (H – A – Y) towers.

II.METHOD OF ANALYSIS

The energy method is a unifying approach to the analysis of both linear and non-linear structures. It is an indirect method of analysis and valid for structures having both small and/or large deformations. The energy method is used to analyze general pin-ended truss and cable structures. By accounting for significant displacements and strains, as well as configuration changes due to structural response, both geometric and material nonlinearities are directly integrated within the formulation [2]. A summary together with step-by-step iterative procedure is presented. The obtained numerical results for all cases are discussed and compared.

The loaded structure's equilibrium position is defined by the point where W "total potential energy" is at its lowest value. Where W is constant for all points. The condition for equilibrium in the i direction at joint j may be expressed as:

$$\frac{\partial W}{\partial x_{ji}} = [g_{ji}] = 0 \qquad ,i = 1,2\ and\ 3 \tag{1}$$

Where: x_{ji}= The displacement of joint j corresponding to a degree of freedom in direction i, and g_{ji} = the corresponding gradient of the energy surface.

By moving down the energy surface along a decent vector v a distance Sv until W is a minimum in that direction gives the location "where W is a minimum.", that is, to a point where:

$$\frac{\partial W}{\partial S} = 0 \tag{2}$$

From this point by using an iterative process, a new descent vector is calculated. The step length S is the length when the descent vector v is a unit vector, along v direction. When v is a unit vector, S will be referred to as the step length for convenience. At the $(k+1)$ iteration, the displacement vector can be expressed as:

$$[x]_{k+1} = [x]_k + S_k v_k \tag{3}$$

Where:

v_k is the descent vector at the K_{th} iteration from x_k in displacement space,

S_k is the step length determining the distance along v_k to the point of $Wmin$.

Summary of the iterative procedures:

The following are the main steps in the iterative processes required to achieve structural equilibrium by minimizing total potential energy:

1. First, before the start of the iteration scheme

a) Calculate the tension coefficients for the pretension forces in the cables by:

$$t_{jn} = \left[\left(T_0 + \frac{EA}{L_0}.e\right)/L_0\right]_{jn} \tag{4}$$

Where:

t_{jn} = the tension force coefficient in member jn,
e = the elongation of cables due to applied load,
T_0 = initial tension in cable due to pretension,

E = /modulus of elasticity,
A = area of the cable element, and
L_0 = the unstrained initial length of the cable.

b) Assume the elements in the initial displacement vector to be zero.

c) Calculate the lengths of all the elements in the pretension structure using the following equation:

$$L_0^2 = \sum_{i=1}^{3} \left(X_{ni} - X_{ji}\right)^2 \quad (5)$$

Where: X = element in displacement vector due to applied load only.

d) For the method of conjugate gradients i, calculate the elements in the scaling matrix:

$$H = diag\{K_{11}^{-1/2}, K_{22}^{-1/2}, \dots, K_{nn}^{-1/2}\} \quad (6)$$

Where:
n = total number of degrees of freedom of all joints,
k = the 12 x 12 stiffness matrix for elements in global coordinates.

2. The steps in the iterative procedure are summarized as:

Step (1) Calculate the elements in the gradient vector of the TPE using:

$$[g_i]_n = \sum_{n=1}^{f_n} \sum_{r=1}^{12} (k_{nr} x_r)_n + \sum_{n=1}^{p_n} t_{jn}\left(X_{ni} - X_{ji} + x_{ni} - x_{ji}\right) - [F_i]_n \quad (7)$$

Step (2) Calculate the Euclidean norm of the gradient vector, $R_k = [g_k^T\, g_k]^{1/2}$ and check if the problem has converged. If $R_k \leq R_{min}$ stop the calculations and print the results. If not, proceed to the next step.

Step (3) Calculate the elements in the descent vector v using:

$$[v]_{k+1} = -[H][g]_{k+1} + \beta_k [v]_k \quad (8)$$

Where; $$[v]_0 = -[g]_0 \quad (9)$$

$$\beta_k = \frac{[g]_{k+1}^T \left[\widehat{K}\right][g]_{k+1}}{[g]_k^T \left[\widehat{K}\right][g]_k} \quad (10)$$

Step (4) Calculate the coefficients in the strep length polynomial from:

$$C_4 = \sum_{n=1}^{P} \left(\frac{EAa_3^2}{2L_0^3}\right)_n \quad (11.a)$$

$$C_3 = \sum_{n=1}^{P} \left(\frac{EAa_2a_3}{L_0^3}\right)_n \quad (11.b)$$

$$C_2 = \sum_{n=1}^{P} \left[t_0 a_3 + \frac{EA(a_2^2 + 2a_1a_3)}{2L_0^3}\right]_n + \sum_{n=1}^{f} \sum_{s=1}^{12} \sum_{r=1}^{12} \left(\frac{1}{2} v_s k_{sr} v_r\right)_n \quad (11.c)$$

$$C_1 = \sum_{n=1}^{P} \left[t_0 a_2 + \frac{EAa_1a_2}{L_0^3}\right]_n + \sum_{n=1}^{f} \sum_{s=1}^{12} \sum_{r=1}^{12} (x_s k_{sr} v_s)_n - \sum_{n=1}^{N} F_n v_n \quad (11.d)$$

Where;

$$a_1 = \sum_{i=1}^{3} \left[\left(X_{ni} - X_{ji}\right) + \frac{1}{2}\left(x_{ni} - x_{ji}\right)\right]\left(x_{ni} - x_{ji}\right) \quad (12.a)$$

$$a_2 = \sum_{i=1}^{3} \left[\left(X_{ni} - X_{ji}\right) + \left(x_{ni} - x_{ji}\right)\right]\left(v_{ni} - xv_{ji}\right) \quad (12.b)$$

$$a_3 = \sum_{i=1}^{3} \left[\frac{1}{2}\left(v_{ni} - v_{ji}\right)^2\right] \quad (12.c)$$

Where;
f = No. of flexural members,
P = No. of pin-jointed members and cables,
F = Element in applied load vector, and
k_{sr} = Element of stiffness matrix in global coordinates of a flexural element.

Step (5) Calculate the step length S using Newton's approximate formula as:

$$S_{k+1} = S_k - \frac{4C_4S^3 + 3C_3S^2 + 2C_2S + C_1}{12C_4S^2 + 6C_3S + 2C_2} \quad (13)$$

Where: k is an iteration suffix and $S_{k=0}$ is taken as zero.

Step (6) Update the tension coefficients using the following equation:

$$\left(t_{jn}\right)_{k+1} = \left(t_{jn}\right)_k + \frac{EA}{\left(L_0^3\right)_{jn}} \left(a_1 + a_2 s + a_3 s^2\right)_{jn} \quad (14)$$

Step (7) Update the displacement vector using equation (4).

Step (8) Repeat the above iteration by returning to step (1).

III.ANALYSIS CONSIDERATIONS

The static analysis is carried out for CSBs having five spans. The bridge has two equal exterior spans of 160 m long each, and three equal interior spans of 320 m long each. The pylons with harp, radiating and semi-fan cable arrangements are shown in Fig. (1).

The pylon is taken as reinforced concrete with hollow rectangular section with properties given in Fig. (2). The top transverse member between the pylons has a reinforced concrete cross section with dimension 1.0 x 1.0 m.

The deck was taken as steel box girder in orthotropic plate shape with properties given in Fig. (3).

The cross girder was taken as built I-section with A=0.12m^2, I_X = 0.0544 m^4, I_Y = 0.0104 m^4, I_P = 0.0648 m^4 and E = 2100 t/cm^2.

The deck girder has a total length of 1280 m and total width of 10 m. Double plane of cables with pylons having H, A and Y shapes are considered which having ten cables on each side of pylons as shown in Fig. (4).

The pylon height relative to the span length of the bridge (H/L) varies between 0.2 and 0.5, with an interval of 0.05. Four common cases of connections between pylon and floor beam are considered as shown in Fig. (5).

The cables were spiral strand bridge cables having a diameter of 13.7 cm with an area of 110.15 cm2, the own weight of 0.089 t/m, the modulus of elasticity of 1472 t/cm^2 and the maximum breaking load of 1506.82 tons. The initial tension of cables in all cases are taken as (5%, 7.5%, 10%, 12.5%, 15%, 17.5%, and 20%) of the maximum breaking load.

The total equivalent live load including impact on the bridge with 10 m as road width is 5.28 t/m for the width of the bridge.

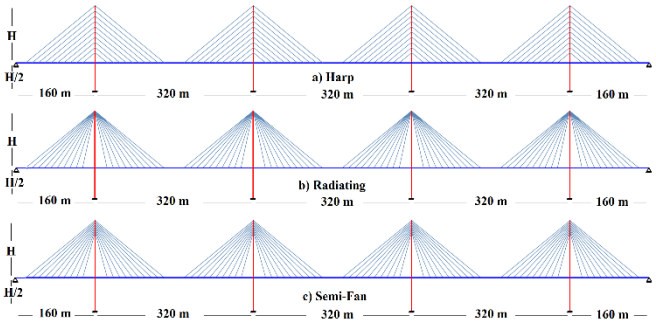

Fig. 1: Five span CSB with various arrangements

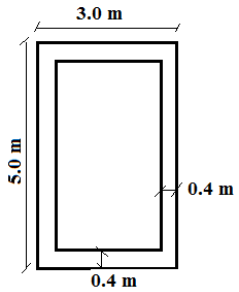

A = 5.76 m^2
I_X = 17.67 m^4
I_Y = 7.52 m^4
I_P = 25.19 m^4
E = 300 t/cm^2
Weight = 14.4 t/m

Fig. 2: Cross sectional properties of pylon

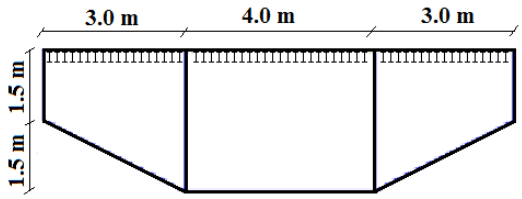

A = 0.625 m^2, I_X = 1.14 m^4, I_Y = 30.5 m^4, I_P = 31.64 m^4,
E = 2100 t/cm^2, D.L = 5.78 t/m, L.L = 5.28 t/m

Fig. 3: Cross sectional properties of floor beam

F

ig. 4: Examples for H, A and Y towers

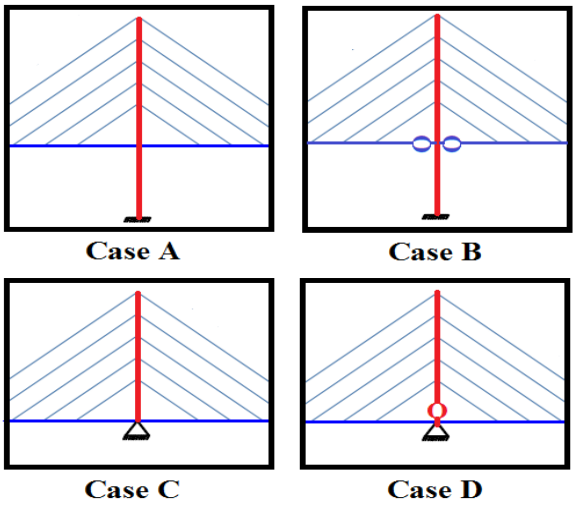

Fig. 5: Four types of connections between pylon and floor beam.

IV.RESULTS AND DISCUSSIONS

In this section, the results for the analysis of the three arrangements of cable-stayed brides including harp, radiating and semi-fan arrangements with different shapes of tower are presented. The variation of maximum response in pylons and floor beams is given in Table (1) and Table (2) respectively. They show that the maximum response in pylon occurs when using harp arrangement, H-Tower, connection type case A, decreasing the initial tension and increasing the height of the pylon. While the maximum response in floor beam occurs when using harp arrangement, Y-Tower, connection type case A, decreasing both the initial tension and the height of the pylon.

Figures (6) to (20) show some of the obtained results for pylon and floor beam.

The relations between the sway ratios (Δ/H) "the maximum lateral displacements at the top of the first pylon to the height of pylons" to the height ratio (H/L) are given in Figs. (6) to (8). Which show that the maximum lateral displacement occurs in Y-tower with harp arrangement.

The relations between the deflection ratios (Δ/L) "the maximum vertical deflection which occurs in the second span to the length of the main span" to the height ratio (H/L) are given in Figs. (9) to (11). Which show that the maximum vertical deflection occurs in Y-tower with harp arrangement.

Figures (12) to (14) contain the variations of normal force along the first pylon, while Figs. (15) to (17) contain the variations of normal force along floor beam. They show that the maximum normal force in pylon occurs in H-Tower with radiating arrangement while the maximum normal force along floor beam occurs in H-Tower with harp arrangement.

The bending moments along the first pylon height and floor beam are given in Figs. (18) to (20) and Figs. (21) to (23) respectively. They show that the maximum bending moment in pylon occurs in H-Tower with harp arrangement while the maximum bending moment along floor beam occurs in A-Tower with radiating arrangement.

Table 1: Maximum response in Pylon

Case Study	Parameter	Max. lateral Displacement (m)	Max. Normal Force (ton)	Max. Bending Moment (m.t)
Arrangement of Cables, H-tower, Case A, To = 12.5%, H/L = 0.4	Harp	0.254	-5053.79	485.32
	Radiating	0.243	-5131.99	133.56
	Semi-Fan	0.245	-4978.97	91.37
Shape of Pylon, Harp, Case A, To = 12.5%	H-Tower	0.254	-5053.79	485.32
	A-Tower	0.199	-5040.06	422.82
	Y-Tower	0.273	-5046.93	360.32
Types of Connection, Harp, H-tower, To = 12.5%, H/L = 0.4	Case A	0.254	-5053.79	485.32
	Case B	0.170	-5040.06	435.32
	Case C	0.220	-4994.63	2860.63
	Case D	0.196	-5040.06	1170.95
To= Initial Tension ratio, Harp, H-tower, Case A, H/L = 0.4	5%	0.372	-4950.68	479.95
	7.5%	0.333	-4985.21	481.51
	10%	0.293	-5019.76	483.95
	12.5%	0.254	-5053.79	485.32
	15%	0.214	-5087.07	488.06
	17.5%	0.175	-5122.17	489.68
	20%	0.135	-5154.76	491.82
Height ratio (H/L), Harp, H-tower, Case A, To = 12.5%	0.20	0.235	-4108.44	597.76
	0.25	0.240	-4339.85	604.57
	0.30	0.244	-4574.11	568.13
	0.35	0.249	-4819.15	526.46
	0.40	0.254	-5053.79	485.32
	0.45	0.256	-5275.84	451.57
	0.50	0.262	-5490.35	416.64

Table 2: Maximum response in Floor beam

Case Study	Parameter	Max. vertical Deflection (m)	Max. Normal Force (ton)	Max. Bending Moment (m.t)
Arrangement of Cables, H-tower, Case A, To = 12.5%, H/L = 0.4	Harp	-0.401	-1574.23	4230.73
	Radiating	-0.373	-1105.28	4392.73
	Semi-Fan	-0.379	-1192.36	4379.80
Shape of Pylon, Harp, Case A, To = 12.5%	H-Tower	-0.401	-1574.23	4230.73
	A-Tower	-0.214	-1542.75	4311.73
	Y-Tower	-0.495	-1511.89	4271.23
Types of Connection, Harp, H-tower, To = 12.5%, H/L = 0.4	Case A	-0.401	-1574.23	4230.73
	Case B	-0.374	-1584.25	4213.01
	Case C	-0.382	-1601.17	4056.91
	Case D	-0.355	-1567.32	4221.81
To= Initial Tension ratio, Harp, H-tower, Case A, H/L = 0.4	5%	-0.682	-1568.23	5214.04
	7.5%	-0.588	-1571.50	4887.03
	10%	-0.495	-1573.75	4560.01
	12.5%	-0.401	-1574.23	4230.73
	15%	-0.307	-1576.99	3902.74
	17.5%	-0.214	-1579.02	3575.14
	20%	-0.120	-1581.04	3243.41
Height ratio (H/L), Harp, H-tower, Case A, To = 12.5%	0.20	-0.930	-3077.37	6435.94
	0.25	-0.691	-2534.47	5431.63
	0.30	-0.550	-2159.35	4824.79
	0.35	-0.460	-1820.12	4474.38
	0.40	-0.401	-1574.23	4230.73
	0.45	-0.360	-1325.89	4090.87
	0.50	-0.330	-1152.51	3982.44

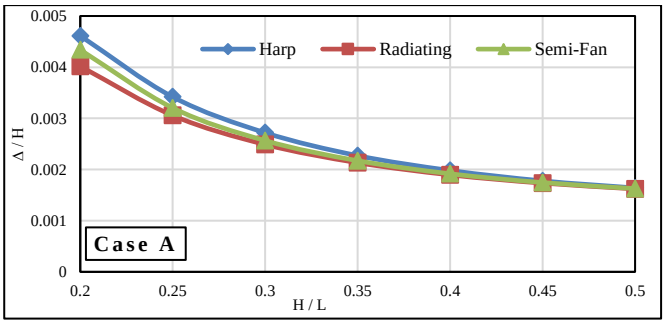

Fig. 6.1: Max. Lateral Displacement at the pylon's top, with various arrangements, Case A

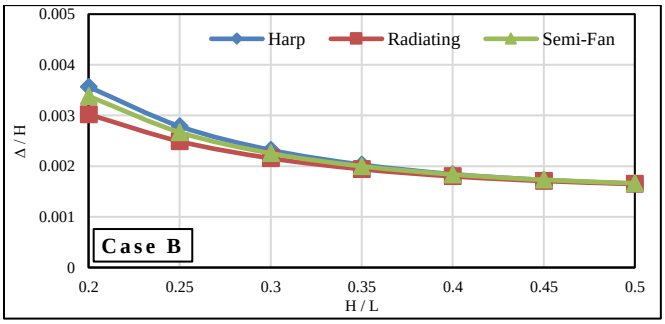

Fig. 6.2: Max. Lateral Displacement at the pylon's top, with various arrangements, Case B

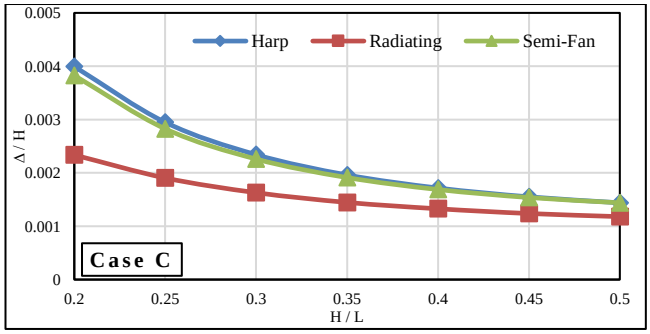

Fig. 6.3: Max. Lateral Displacement at the pylon's top, with various arrangements, Case C

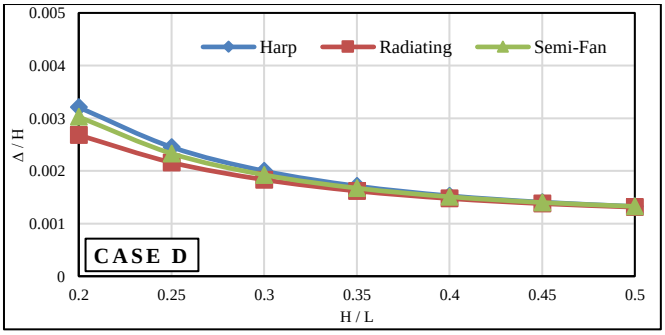

Fig. 6.4: Max. Lateral Displacement at the pylon's top, with various arrangements, Case D

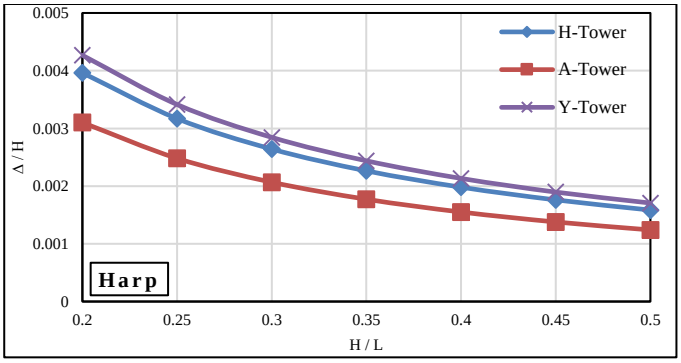

Fig. 7.1: Max. Lateral Displacement at the pylon's top, with various Pylons, Case A, Harp

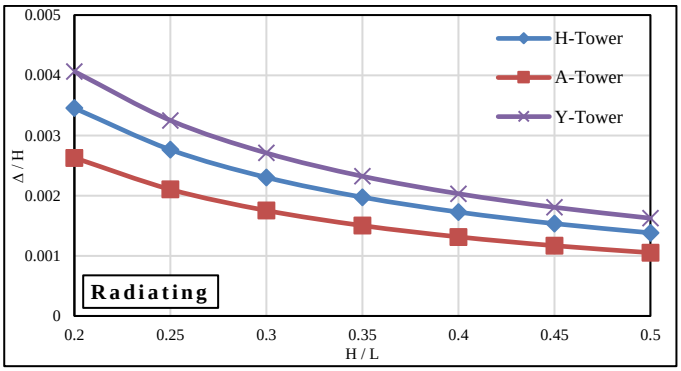

Fig. 7.2: Max. Lateral Displacement at the pylon's top, with various Pylons, Case A, Radiating

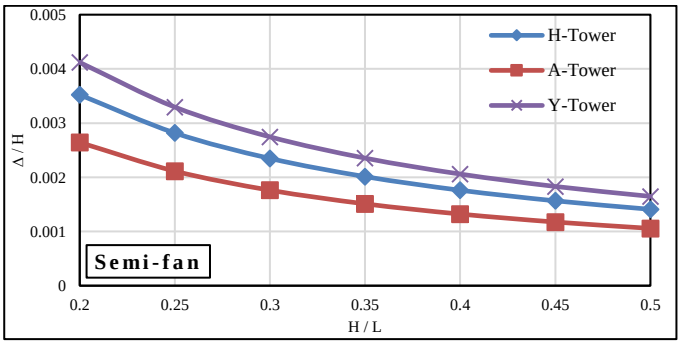

Fig. 7.3: Max. Lateral Displacement at the pylon's top, with various Pylons, Case A, Semi-Fan

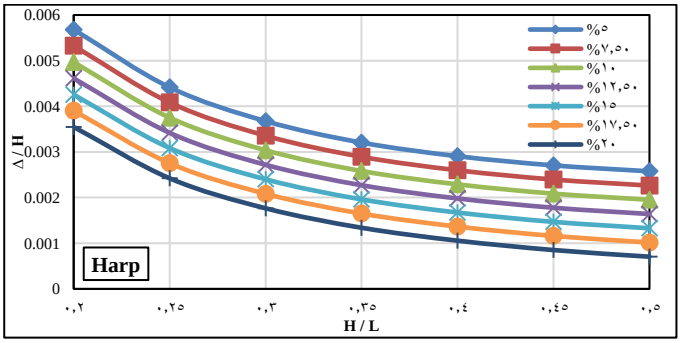

Fig. 8.1: Max. Lateral Displacement at the pylon's top, with various initial tension, Case A, Harp

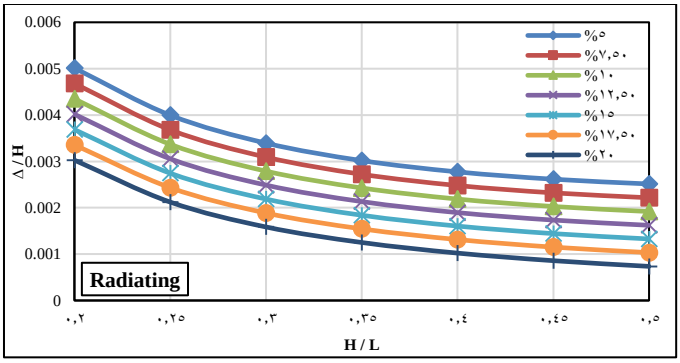

Fig. 8.2: Max. Lateral Displacement at the pylon's top, with various initial tension, Case A, Radiating

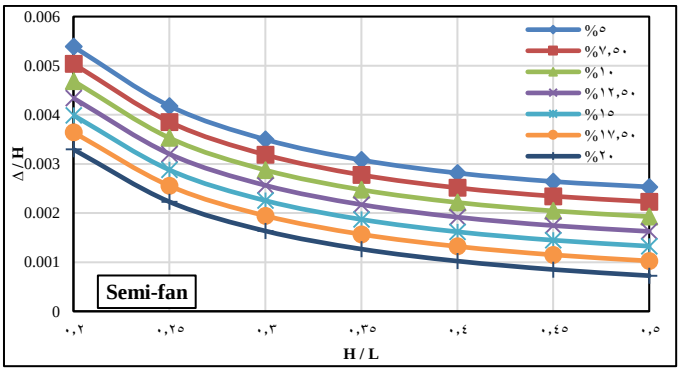

Fig. 8.3: Max. Lateral Displacement at the pylon's top, with various initial tension, Case A, Radiating

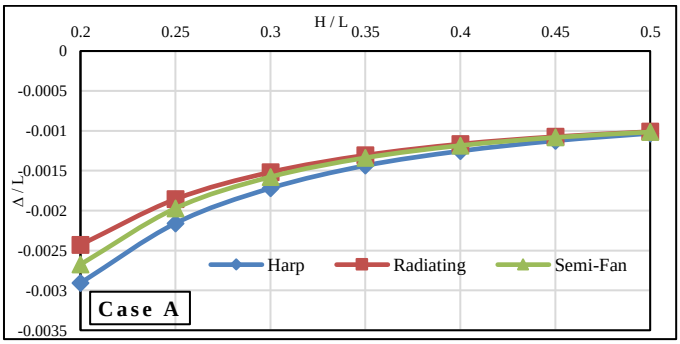

Fig. 9.1: Max. Vertical Deflection at floor beam, with various arrangements, Case A

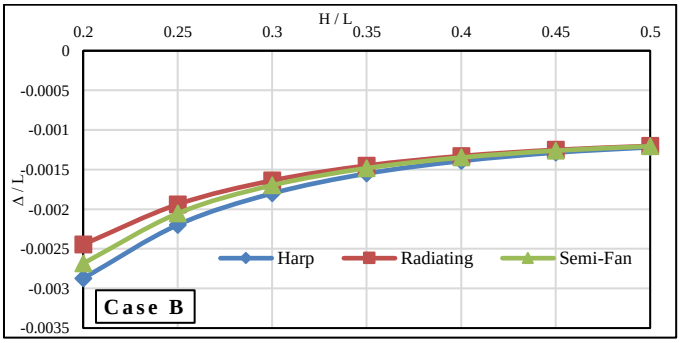

Fig. 9.2: Max. Vertical Deflection at floor beam, with various arrangements, Case B

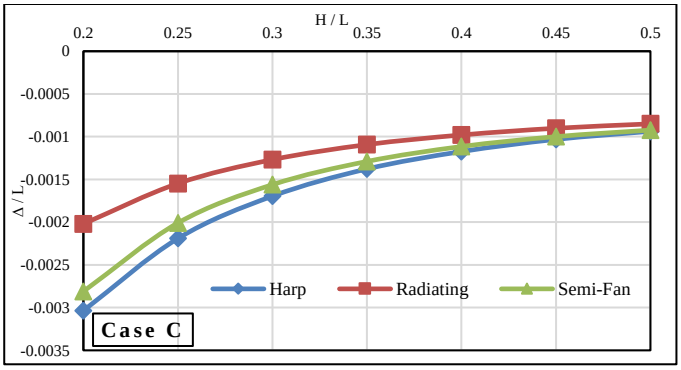

Fig. 9.3: Max. Vertical Deflection at floor beam, with various arrangements, Case C

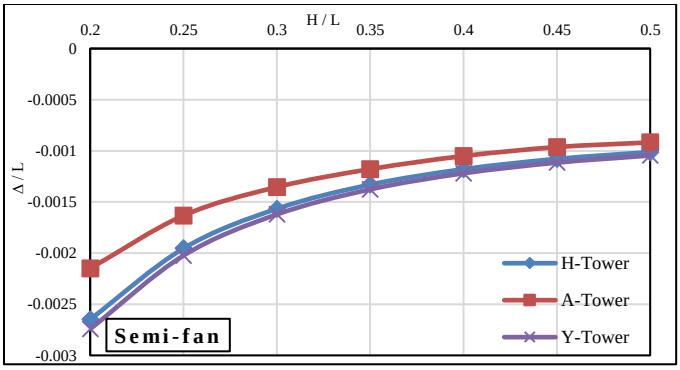

Fig. 10.3: Max. Vertical Deflection at floor beam, with various Pylons, Case A, Semi-Fan

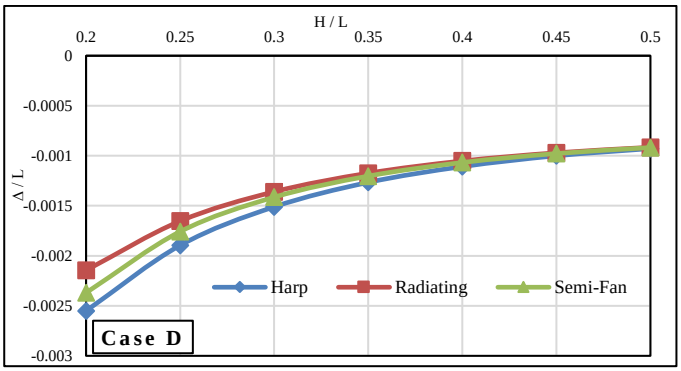

Fig. 9.4: Max. Vertical Deflection at floor beam, with various arrangements, Case D

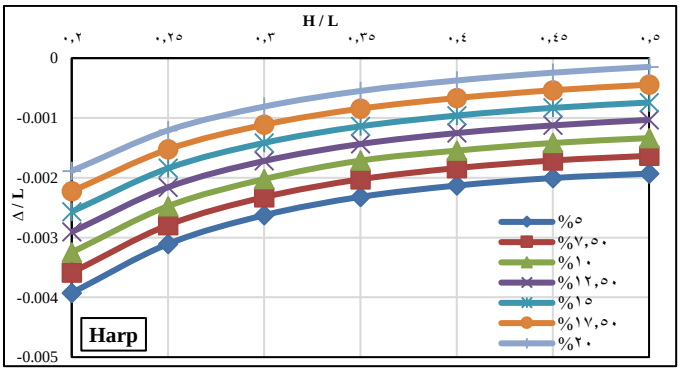

Fig. 11.1: Max. Vertical Deflection at floor beam, with various Initial tension, Case A, Harp

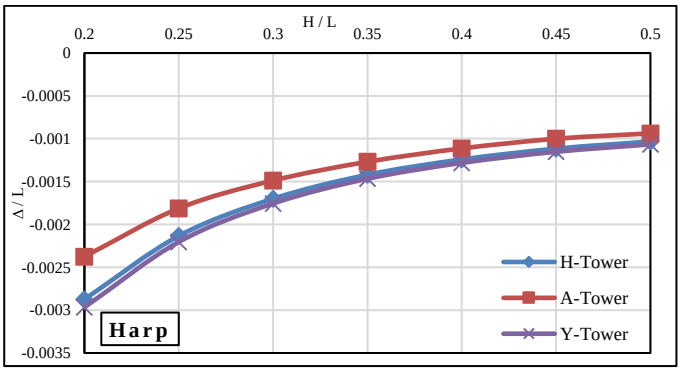

Fig. 10.1: Max. Vertical Deflection at floor beam, with various Pylons, Case A, Harp

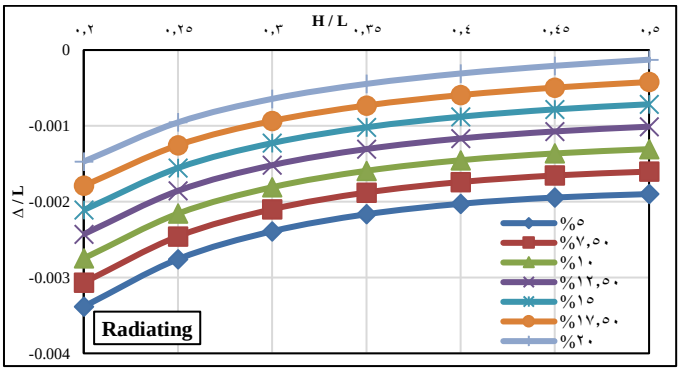

Fig. 11.2: Max. Vertical Deflection at floor beam, with various Initial tension, Case A, Radiating

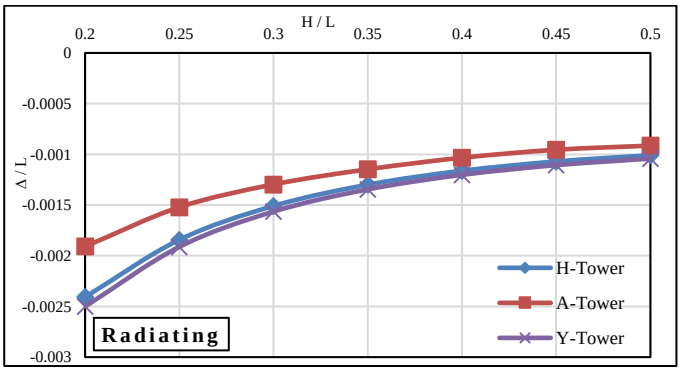

Fig. 10.2: Max. Vertical Deflection at floor beam, with various Pylons, Case A, Radiating

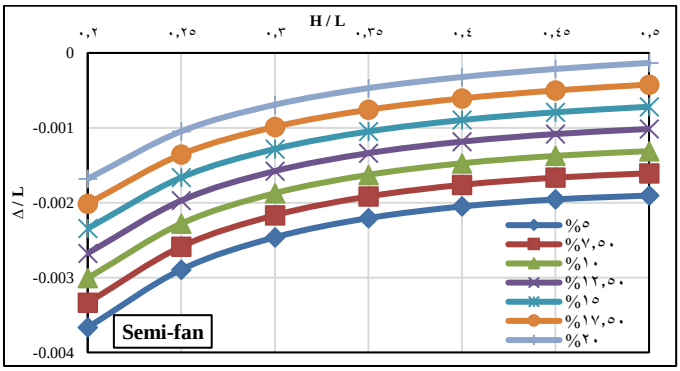

Fig. 11.3: Max. Vertical Deflection at floor beam, with various Initial tension, Case A, Semi-Fan

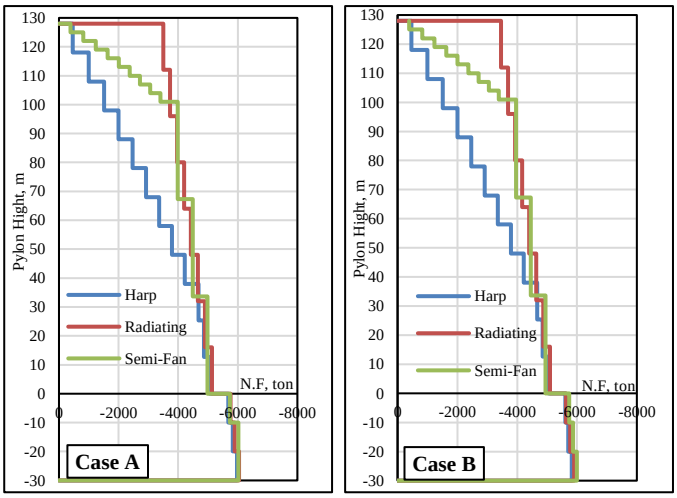

Fig. 12.1: Normal Force along Pylon, with various arrangements, Case A and Case B

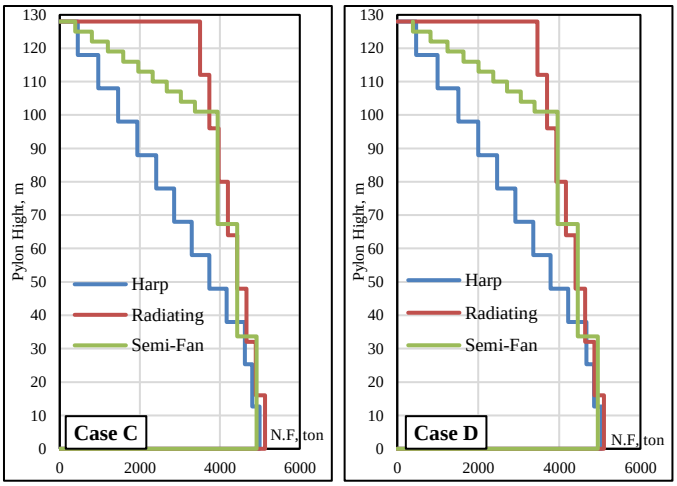

Fig. 12.2: Normal Force along Pylon, with various arrangements, Case C and Case D

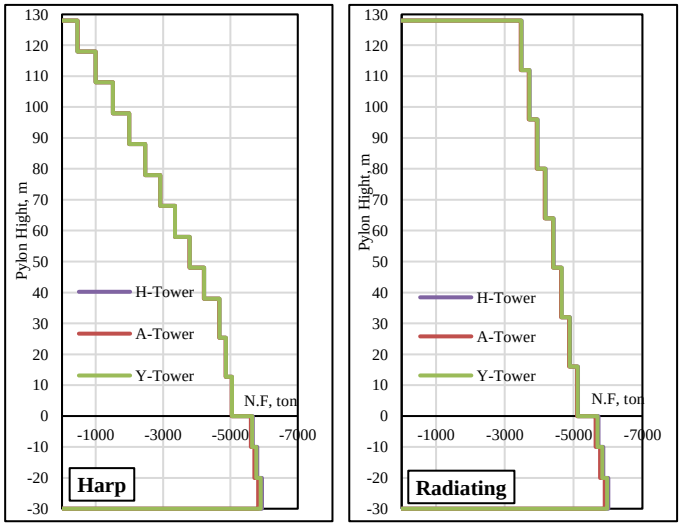

Fig. 13.1: Normal Force along Pylon Height, with various Pylons, Case A, Harp and Radiating

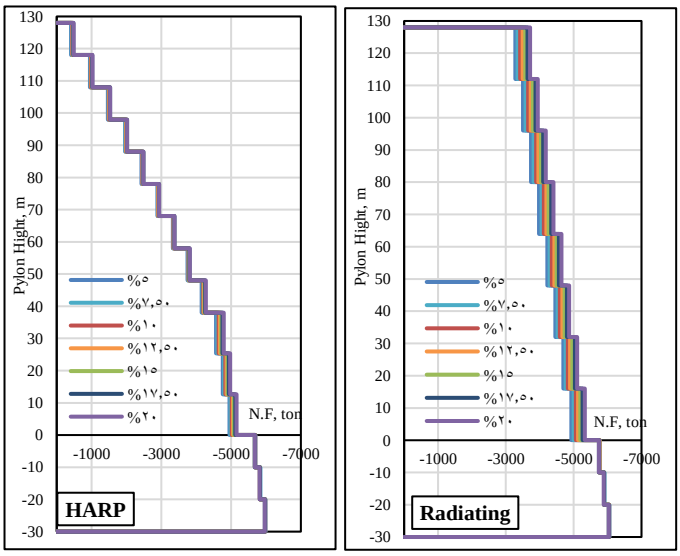

Fig. 14.1: Normal Force along Pylon Height, with various initial tension, Case A, Harp and Radiating

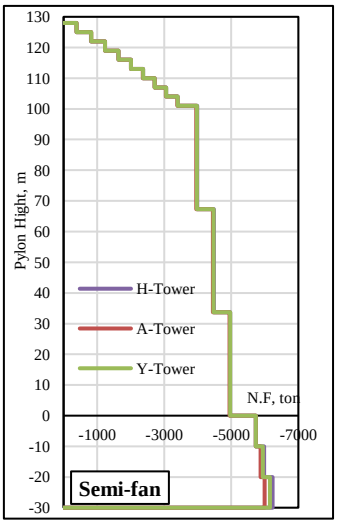

Fig. 13.2: Normal Force along Pylon Height, with various Pylons, Case A, Semi-fan

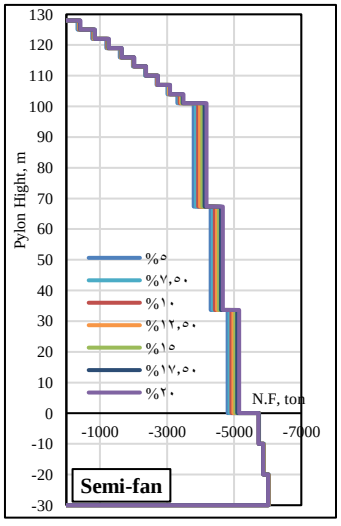

Fig. 14.2: Normal Force along Pylon Height, with various initial tension, Case A, Semi-fan

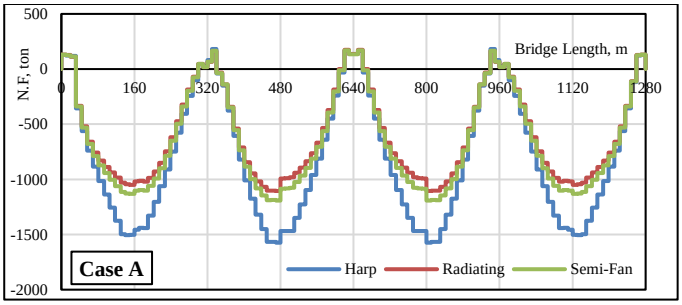

Fig. 15.1: Normal Force along floor beam, with various arrangements, Case A

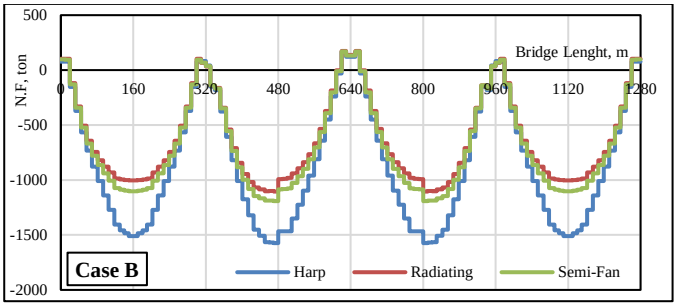

Fig. 15.2: Normal Force along floor beam, with various arrangements, Case B

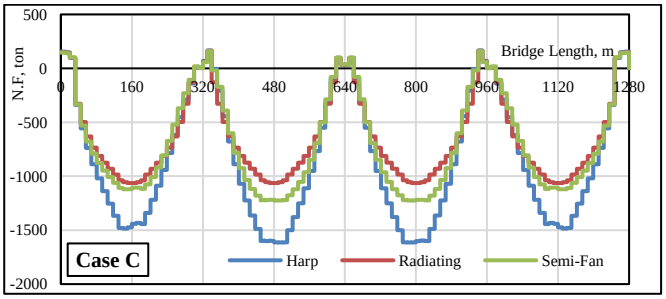

Fig. 15.3: Normal Force along floor beam, with various arrangements, Case C

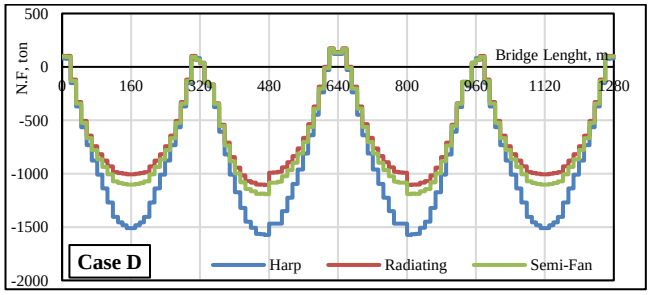

Fig. 15.4: Normal Force along floor beam, with various arrangements, Case D

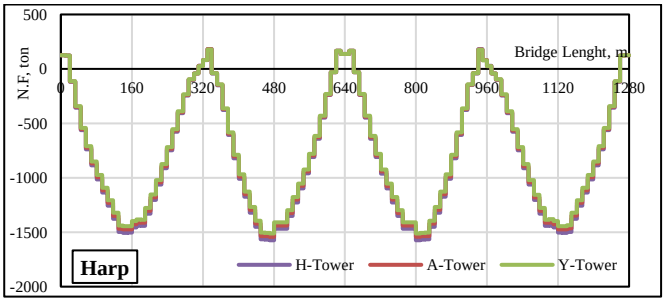

Fig. 16.1: Normal Force along floor beam, with various Pylons, Case A, Harp

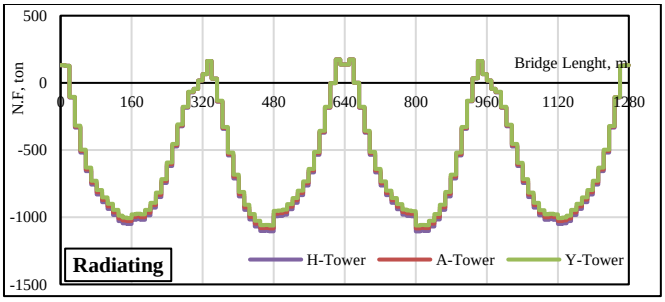

Fig. 16.2: Normal Force along floor beam, with various Pylons, Case A, Radiating

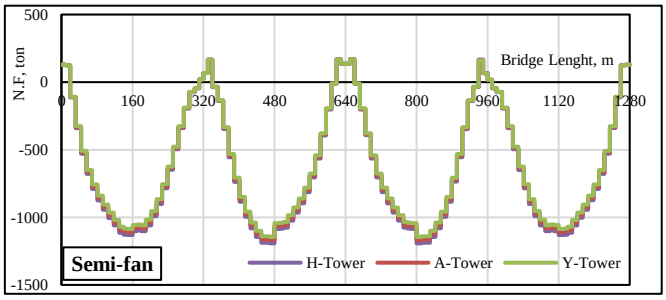

Fig. 16.3: Normal Force along floor beam, with various Pylons, Case A, Semi-fan

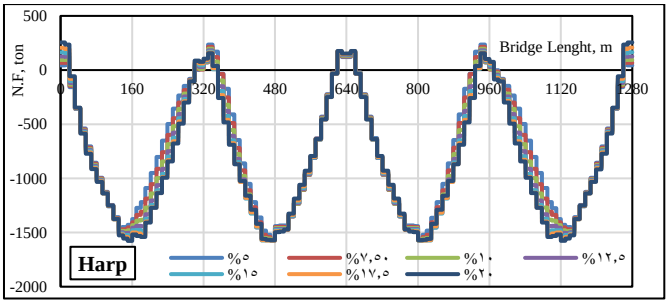

Fig. 17.1: Normal Force along floor beam, with various initial tension, Case A, Harp

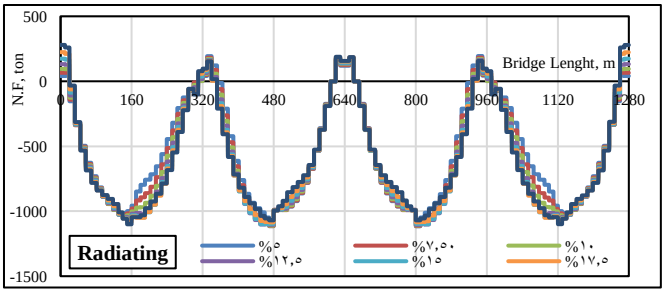

Fig. 17.2: Normal Force along floor beam, with various initial tension, Case A, Radiating

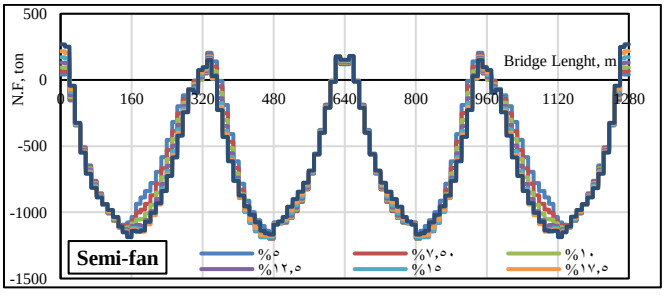

Fig. 17.3: Normal Force along floor beam, with various initial tension, Case A, Semi-fan

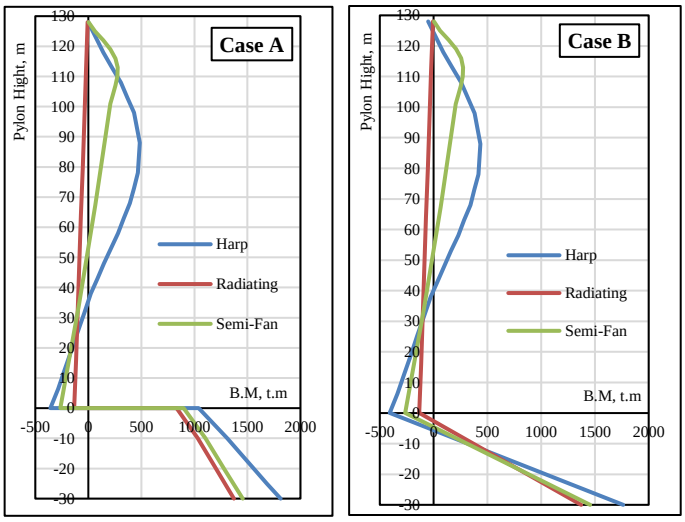

Fig. 18.1: Bending Moment along Pylon, with various arrangements, Case A and Case B

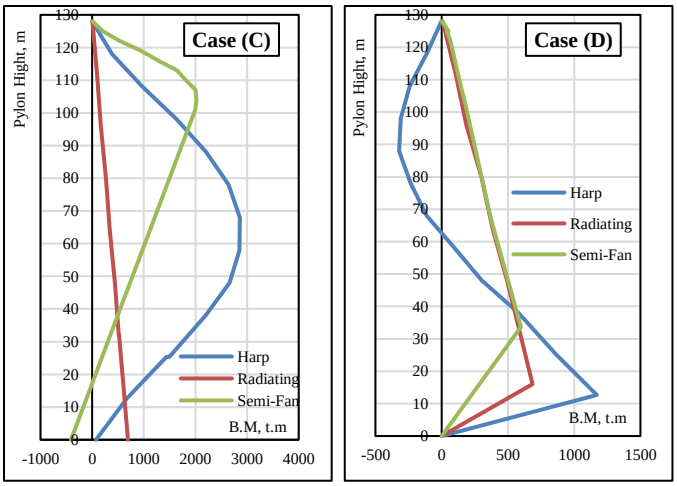

Fig. 18.2: Bending Moment along Pylon, with various arrangements, Case C and Case D

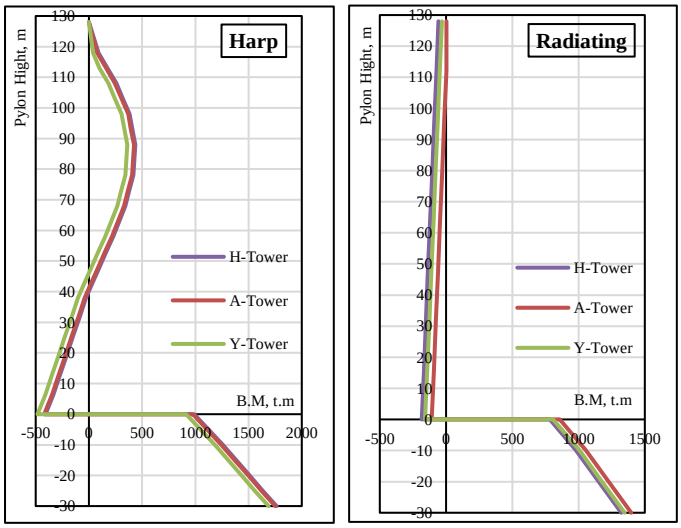

Fig. 19.1: Bending Moment along Pylon Height, with various Pylons, Case A, Harp and Radiating

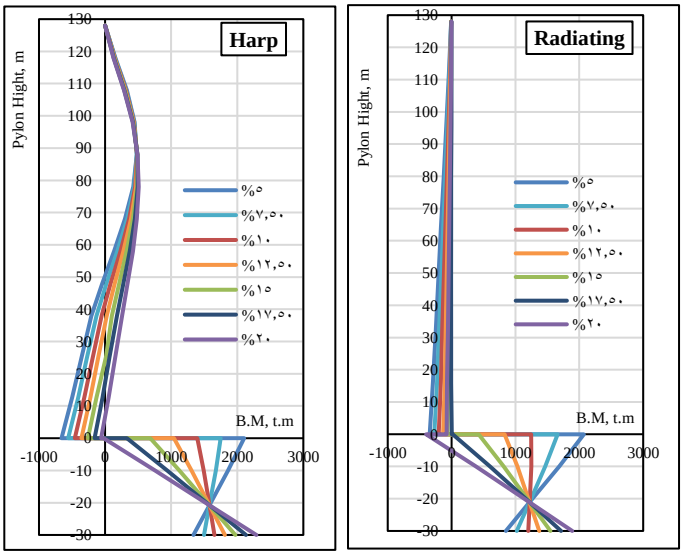

Fig. 20.1: Normal Force along Pylon Height, with various initial tension, Case A, Harp and Radiating

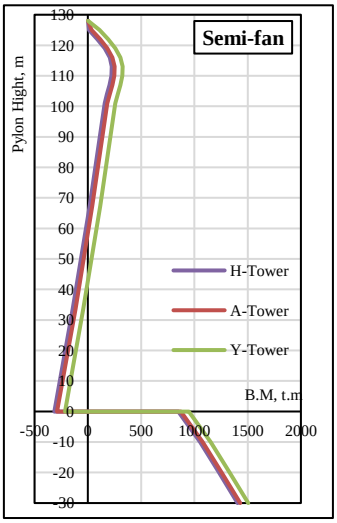

Fig. 19.2: Bending Moment along Pylon Height, with various Pylons, Case A, Semi-fan

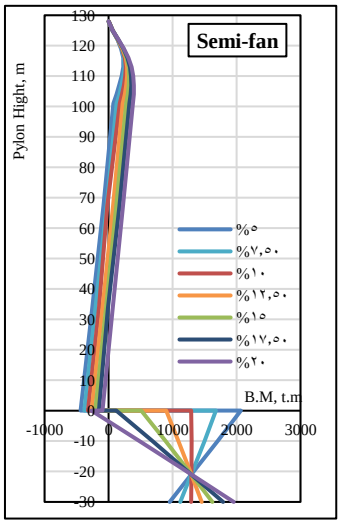

Fig. 20.2: Normal Force along Pylon Height, with various initial tension, Case A, Semi-fan

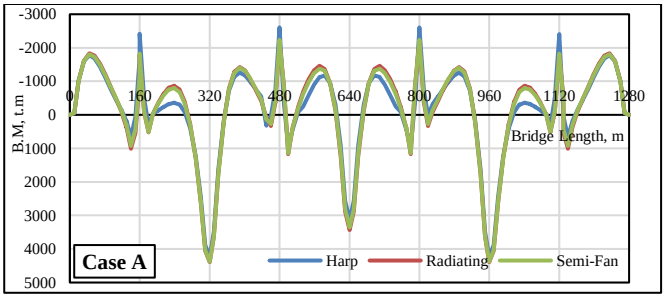

Fig. 21.1: Bending Moment along floor beam, with various arrangements, Case A

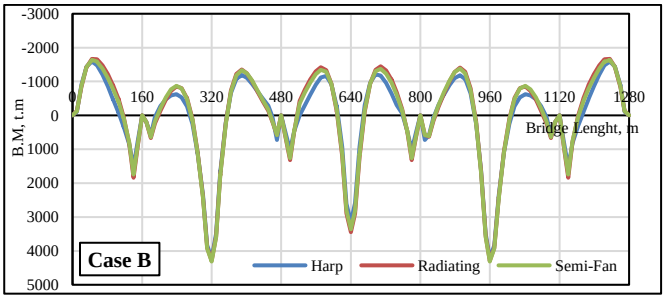

Fig. 21.2: Bending Moment along floor beam, with various arrangements, Case B

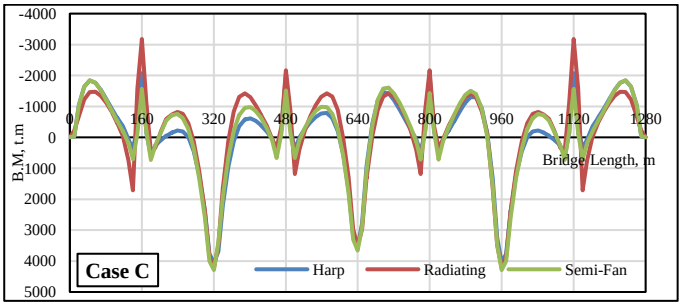

Fig. 21.3: Bending Moment along floor beam, with various arrangements, Case C

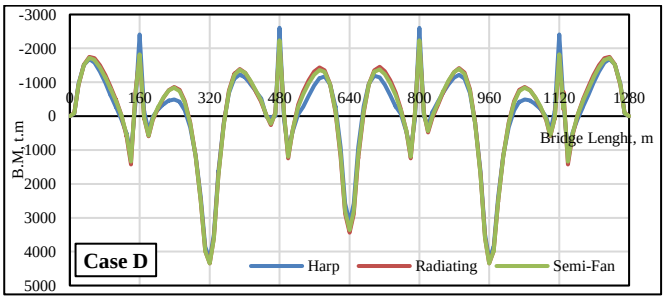

Fig. 21.4: Bending Moment along floor beam, with various arrangements, Case D

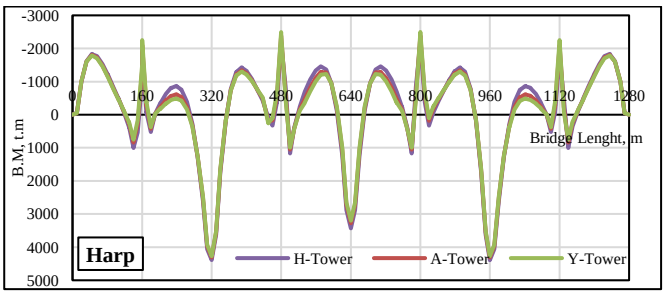

Fig. 22.1: Bending Moment along floor beam, with various Pylons, Case A, Harp

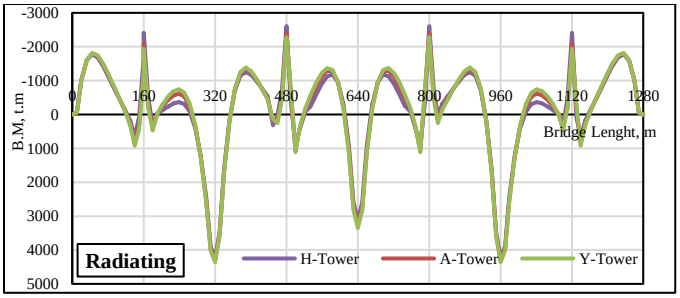

Fig. 22.2: Bending Moment along floor beam, with various Pylons, Case A, Radiating

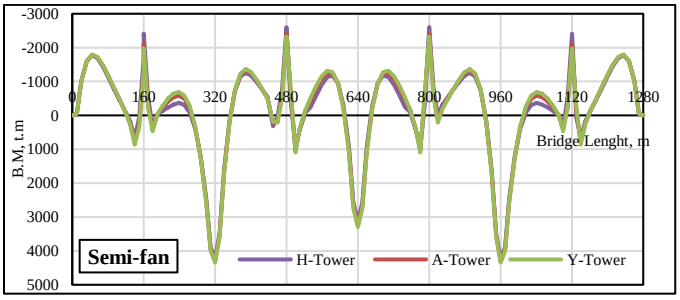

Fig. 22.3: Bending Moment along floor beam, with various Pylons, Case A, Semi-fan

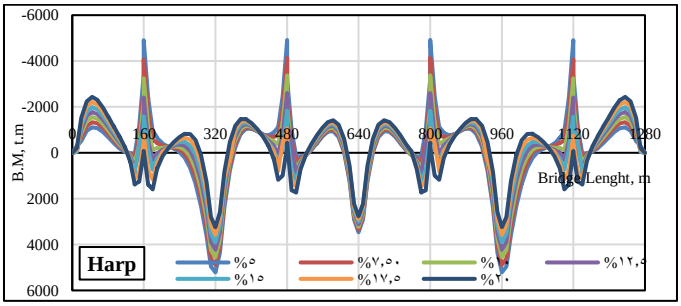

Fig. 23.1: Bending Moment along floor beam, with various initial tension, Case A, Harp

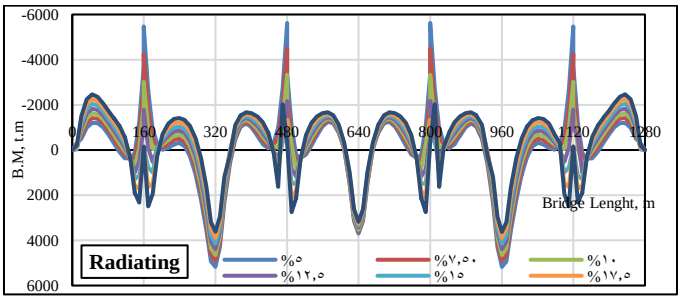

Fig. 23.2: Bending Moment along floor beam, with various initial tension, Case A, Radiating

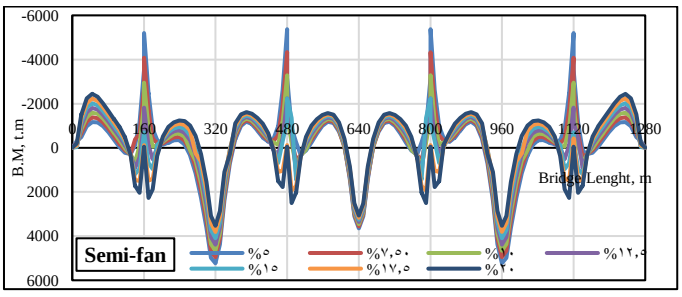

Fig. 23.3: Bending Moment along floor beam, with various initial tension, Case A, Semi-fan

V.CONCLUSIONS

In this paper, various cases along with dead load and live load for the different cable arrangement with H, A and Y shape tower for analysis have been considered. Following are the conclusions of this study:

1. Radiating shape decreases the lateral displacement of the pylon by 5% and the maximum deflection of the floor beam by 7%, but it has the maximum normal force along the pylon height.

2. The A-tower is more effective in decreasing both the lateral displacement of the pylon by 17% and the vertical deflection of the floor beam by 57%.

3. The connection type between pylons and floor beam has a significant influence on all various responses. In all phases of comparisons, the connection type case B is the best choice.

4. Increasing the height ratio (H/L) causes an increase for the lateral displacement and the normal force of the pylon although it decreases the bending moment along the pylon height, the deflection, moment and normal force in the floor beam.

5. Increasing the pretension forces in cables decreases the lateral displacement of pylons, vertical deflection and bending moment of floor beam but increases the normal force along floor beam. Also, the normal force and bending moment of the pylon increases.

REFERENCES

[1] Buchholdt, H. A., ″ an Introduction to Cable Roof Structures″, Cambridge University Press, 1985.

[2] Naguib, M. “Single and Double Planes of Cables in Harp Cable Stayed Bridges”, Mansoura Engineering Journal (MEJ), Vol. 30, No. 3, September 2005.

[3] Troitsky, M. S., “Cable- Stayed Bridges, Theory and Design”, Crosby Lockwood Staples, London, 2nd ed., 1989.

[4] Naguib, M. “Influence of Connections between towers and Floor Beams in Cable-Supported towers and Floor Beams in Cable-Supported Bridges”, Mansoura Engineering Journal (MEJ), Vol. 28, No. 4, December 2003.

[5] Stefanou, G. D., Moossavi, E., Bishop, S., and Koliopoulos, P., “ Conjugate gradients for calculating the response of large cable nets to static loads” Computers & Structures, Vol. 49, No.5, pp. 843-848, 1993.

[6] Buchholdt, H. A., “Tension structures”, Struc. Engrg., Vol. 48, No. 2, pp. 45-54., February 1970.

[7] Naguib, M., “Two Spans Cable Stayed Bridges”, Mansoura Engineering Journal (MEJ), Vol. 30, No. 4, December2005.

[8] G. M. Savaliya, “Static and Dynamic Analysis of Cable-Stayed Suspension Hybrid Bridge & Validation” IJARET, Volume 6, Issue 11, Nov 2015, pp. 91-98.

[9] Shivanshi and Pinaki, “Analysis of the Behaviour of Cable Stayed Bridge with Different Types of Cables Arrangement” IJIERE, Volume 3, Issue 5, 2016

[10] Mycherla Chaitanya and M. Ramakrishna, “Modelling & Comparative Analysis of Cable Stayed & Girder Bridges using SAP2000” IJRASET, Volume 6, Issue 2, February 2018.

[11] Hiram Arellano, Roberto Gomez, Dante Tolentino, “Parametric Analysis of Multi-Span Cable-Stayed Bridges under Alternate Loads”, The Baltic Journal of Road and Bridge Engineering, Volume 14, Issue 4, 2019

[12] Abhishek Pandey, Nitesh Kushwah,“Seismic Analysis and Design of Cable Stayed Bridge with Different Cable Arrangements” IRJET, Volume 7, Issue 12, December 2020.